The eclipsing massive X-ray binary M33 X−7: New X-ray observations and optical identification[*]

W. Pietsch[1], B. J. Mochejska[2,3], Z. Misanovic[1], F. Haberl[1], M. Ehle[4], and G. Trinchieri[5]

[1] Max-Planck-Institut für extraterrestrische Physik, 85741 Garching, Germany
[2] Harvard-Smithsonian Center for Astrophysics, 60 Garden Street, Cambridge, MA 02138, US
[3] Hubble Fellow
[4] XMM-Newton Science Operations Centre, ESA, Villafranca del Castillo, P.O. Box 50727, 28080 Madrid, Spain
[5] Osservatorio Astronomico di Brera, via Brera 28, 20121 Milano, Italy

Abstract. The eclipsing X-ray binary M33 X−7 was in the field of view during several observations of our XMM-Newton M33 survey and in the archival *Chandra* observation 1730 which cover a large part of the 3.45 d orbital period. We detect emission of M33 X−7 during eclipse and a soft X-ray spectrum of the source out of eclipse that can best be described by bremsstrahlung or disk blackbody models. No significant regular pulsations of the source in the range 0.25–1000 s were found. The average source luminosity out of eclipse is 5×10^{37} erg s^{-1} (0.5–4.5 keV). In a special analysis of DIRECT observations we identify as optical counterpart a B0I to O7I star of 18.89 mag in V which shows the ellipsoidal heating light curve of a high mass X-ray binary with the M33 X−7 binary period. The location of the X-ray eclipse and the optical minima allow us to determine an improved binary period and ephemeris of mid-eclipse as HJD $(245\,1760.61 \pm 0.09) \pm N \times (3.45376 \pm 0.00021)$. The mass of the compact object derived from orbital parameters and the optical companion mass, the lack of pulsations, and the X-ray spectrum of M33 X−7 may indicate that the compact object in the system is a black hole. M33 X−7 would be the first detected eclipsing high mass black hole X-ray binary.

Key words. Galaxies: individual: M33 - X-rays: individuals: M33 X−7 - X-rays: binaries - binaries: eclipsing

1. Introduction

M33 X−7 (hereafter X−7) was detected as a variable source with a luminosity brighter than 10^{38} erg s^{-1} in *Einstein* observations (Long et al. 1981; Markert & Rallis 1983; Trinchieri et al. 1988a,b). Peres et al. (1989) suggested that the X−7 variability pattern can be explained by an eclipsing X-ray binary (XRB) with an orbital period of 1.7 d and an eclipse duration of ∼ 0.4 d. This finding was the first identification of a close accreting binary system with an X-ray source in an external galaxy other than the Magellanic Clouds. It was confirmed combining *Einstein* observatory and first ROSAT data (Schulman et al. 1993, 1994). With the inclusion of more ROSAT and ASCA data (Larson & Schulman 1997; Dubus et al. 1999, hereafter D99) the orbital period turned out to be twice as long. The shape of the eclipse could be described by a slow ingress ($\Delta\Phi_{\mathrm{ingress}} = 0.10 \pm 0.05$), an eclipse duration of $\Delta\Phi_{\mathrm{eclipse}} = 0.20 \pm 0.03$, and a fast eclipse egress ($\Delta\Phi_{\mathrm{egress}} = 0.01 \pm 0.01$) with an ephemeris for the mid-eclipse

time of HJD $244\,8631.5 \pm 0.1 + N \times (3.4535 \pm 0.0005)$. In addition, D99 discovered evidence for a 0.31 s pulse period. The orbital period, pulse period and observed X-ray luminosity are remarkably similar to those of the Small Magellanic Cloud neutron star XRB SMC X−1 (Liu et al. 2000). However, if the pulse period of X−7 can not be confirmed, the source could also resemble high mass black hole XRBs (BHXB) like LMC X−1 or LMC X−3. It would be the first eclipsing object within this rare class of XRBs.

The position of X−7 correlates with the dense O–B association HS13 (Humphreys & Sandage 1980) and therefore no individual counterpart could be identified based on position only. However, its location in HS13 is consistent with the expectation of a massive companion. As D99 point out, the optical counterpart is likely to show ellipsoidal and/or X-ray heating variations (Tjemkes et al. 1986) which can be used for the optical identification.

Variable optical sources within M33 were systematically searched for in the DIRECT project (see e.g. Mochejska et al. 2001b, hereafter M01b). Many eclipsing binaries, Cepheids, and other periodic, possibly long-period or nonperiodic variables were detected. X−7 is located in DIRECT field M33B. The variability of the optical counterpart was not detected in the

previous analysis due to the limitations of the variable search strategy for such small amplitude variables in crowded regions.

As a follow-up of our study of the X-ray source population of M33 based on all archival ROSAT observations (Haberl & Pietsch 2001, hereafter HP01), we planned a deep XMM-Newton raster survey of M33 based on 22 Telescope Scientist guaranteed time (proposal no 010264) and AO2 (proposal no 014198) observations, each with a duration of about 10 ks (for first results see Pietsch et al. 2003). X−7 was covered in 13 of these observations at varying off-axis angles and covering different orbital phases.

In this paper we report on time and spectral variability of X−7 within the XMM-Newton raster survey. We add results from an archival *Chandra* observation, which covered the source, and a dedicated timing analysis of the DIRECT data of the HS13 region.

2. X-ray observations and results

For the detailed analysis of X−7 we mostly used data from XMM-Newton EPIC. From the M33 observations in the *Chandra* archive only the observation with identification no 1730 covered the X−7 field. Table 1 summarizes the observation identifications (Col. 1), observation dates (2), elapse time (3), extraction radius $R_{\rm ext}$ used for count rates, light curves, and spectra (4), X−7 raw count rates in the 0.5–4.5 keV band (5), hardness ratios (6), and luminosities in the 0.5–4.5 keV band (7). For the XMM-Newton observations, values in columns 4 to 7 correspond to the EPIC PN detector if not indicated differently, since it gives about twice the number of photons than the EPIC MOS cameras. Off axis angle of X−7 (8) and phase coverage within the binary orbit according to the ephemeris of D99 (9) are also given. As hardness ratio (HR) we use the ratio of the counts in the 1.2–3.0 keV band to the counts in the 0.5–1.2 keV band. Luminosities were determined from thermal bremsstrahlung spectra (see Sect. 2.3). During observations 0102640101 and 0102641101 X−7 was in low state and source statistics did not allow us to derive hardness ratios. For these observations we assumed that the source spectrum was similar to the spectrum during observation 0102642301 and scaled the source luminosity from the vignetting corrected count rates.

In the XMM-Newton observations (Jansen et al. 2001) the EPIC PN and MOS instruments (Strüder et al. 2001; Turner et al. 2001) were mostly operated in the full frame mode resulting in a time resolution of 73.4 ms and 2.6 s, respectively. Only for the first two observations in Table 1, the PN detector was operated in the extended full frame mode (time resolution 200 ms) and during observation 0102640101 the MOS detectors were operated in the small window mode (0.3 s time resolution for the inner CCDs). The medium filter was in front of the EPIC cameras in all but the first two observations which were performed with the thick filter. We used all EPIC instruments for imaging, position determination and for the timing and spectral investigations of X−7. In most of the observations the source is located at high off-axis angle (see Table 1), and could be outside of the field of view in some of the cameras. Also, the cameras normally cover different times. The XMM-Newton point spread function (PSF) required extraction radii
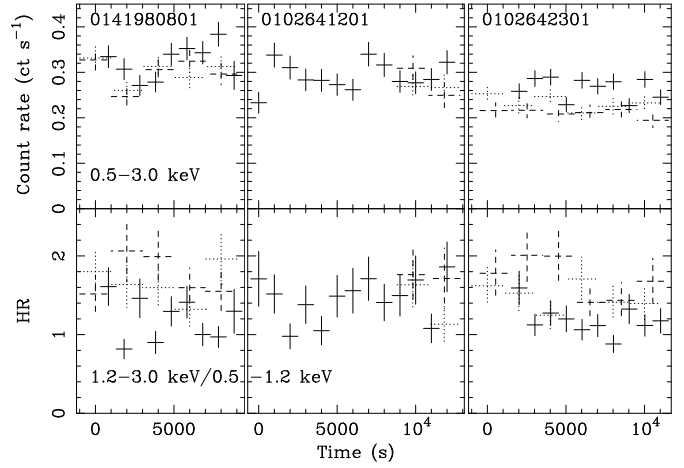

Fig. 1. XMM-Newton EPIC light curves and hardness ratio of M33 X−7 during observations 0141980801, 0102641201, and 102642301 with time zero corresponding to HJD 245 2683.14827, 245 1758.79473, 245 2301.91542, respectively (solar system barycenter corrected). Count rates were corrected for vignetting. EPIC MOS rates were scaled by a factor of 2.5 to approximately correct for the difference in instrument efficiency compared to EPIC PN. EPIC PN, MOS1 and MOS2 data are marked with solid, dotted, and dashed error bars. The light curves cover orbital phases 0.20–0.23, 0.54–0.58, and 0.81–0.85 (left to right, ephemeris of D99).

$R_{\rm ext}$ larger than 22″5 to encircle > 80% of the source photons. Depending on the location of the source, counts could be missing due to CCD gaps. Many of the XMM-Newton observations suffer from times of high particle background. To be able to also use these times to cover as much as possible of the X−7 binary orbit, we restricted the energy band for light curve and hardness ratio analysis to 0.5–3.0 keV where the source is brightest.

Four *Chandra* ACIS observations (Weisskopf et al. 2000) of M33 were obtained from the *Chandra* Data Archive (http://asc.harvard.edu/cgi-gen/cda). However, only the ACIS I observation 1730 (see Table 1) covered the X−7 field. The instrument was operated in the full frame mode (3.2 s time resolution). X−7 is positioned in the outer corner of the front-illuminated CCD chip I2 during the observation.

The deep space orbits of the satellites XMM-Newton and *Chandra* led to long continuous observation times of X−7. The low earth orbits of the *Einstein*, ROSAT, ASCA and *Beppo*SAX observatories on the other hand, led to observations split in many short intervals of typically less than 1 500 s.

The data analysis was performed using tools in the SAS v5.4.0, CIAO v2.3, EXSAS/MIDAS 1.2/1.4, and FTOOLS v5.2 software packages, the imaging application DS9 v2.1b4 , the timing analysis package XRONOS v5.19 and spectral analysis software XSPEC v11.2.

For the time variability investigations all X−7 event times were corrected to solar system barycenter arrival times.

2.1. Time variability

The X-ray light curve of X−7 was sampled with a time resolution of 1000 s for EPIC PN and with 2000 s for MOS. While

Table 1. M33 X−7 observations with the observatories XMM-Newton (proposal numbers 010264 and 014198) and *Chandra* (1730). Besides observation 0102642101, where M33 X−7 was only in the field of view of the MOS detectors, for XMM-Newton we give EPIC PN count rates, hardness ratios and luminosities. For the low state observations, no hardness ratio could be determined.

Obs. id.	Obs. dates	Elapse time (ks)	R_{ext} ($''$)	Count rate** (ct ks^{-1})	HR	L_X^{**} (10^{37} erg s^{-1})	Offax ($'$)	Binary phase
(1)	(2)	(3)	(4)	(5)	(6)	(7)	(8)	(9)
0102641201	2000-08-02	13.1	30.0	172 ± 4	1.40 ± 0.38[†]	8.7	10.4	0.54–0.58
0102640401	2000-08-02	13.1	40.0	163 ± 5	1.27 ± 0.23[†]	8.5	10.4	0.61–0.66
0102640101	2000-08-04	13.3	22.5	4.0 ± 1.2		0.2	8.3	0.11–0.16
0102640501	2001-07-05	11.8	45.0	57 ± 2	1.27 ± 0.30	8.3	7.1	0.33–0.36
0102640601	2001-07-05	8.2[+]	35.0	75 ± 5	1.09 ± 0.45	6.0	15.7	0.23–0.26
0102640701	2001-07-05	11.7	35.0	54 ± 2	1.10 ± 0.26	7.8	9.3	0.28–0.31
0102541101	2001-07-08	12.5	30.0	5.1 ± 1.7		0.3	11.1	0.01–0.05
0102642101	2002-01-25	12.3*	35.0	115 ± 3*	1.61 ± 0.35*	8.5	13.1	0.25–0.29
0102642301	2002-01-27	12.3	35.0	316 ± 6	1.17 ± 0.20	7.0	0.9	0.81–0.85
0141980501	2003-01-22	8.1	35.0	114 ± 10	1.20 ± 0.15	9.0	8.3	0.18–0.21
0141980601	2003-01-23	13.6	37.5	153 ± 4	1.23 ± 0.28	7.3	10.4	0.46–0.50
0141980701	2003-01-24	13.7	35.0	164 ± 6	1.12 ± 0.34	7.3	10.4	0.52–0.56
0141980801	2003-02-12	10.2	35.0	221 ± 6	1.16 ± 0.28	8.6	8.3	0.20–0.23
1730	2000-12-07	52.0	15.0	100 ± 2	1.89 ± 0.09	6.3	8.6	0.49–0.65

Notes and references:

[+] : M33 X−7 only in PN field of view.

* : M33 X−7 only in MOS field of view, integrated MOS count rate, hardness ratio and luminosity given.

[†] : The on average higher HR during observations 0102641201 and 0102640401 compared to the other observations reflects the difference between thick and medium filter and most likely not a change of the spectrum of M33 X−7.

**: raw count rate and luminosity in the 0.5–4.5 keV band assuming the best fitting thermal bremsstrahlung spectrum (see Table 3) corrected for a Galactic foreground absorption of $N_H = 6.38 \times 10^{20}$ cm^{-2} (Dickey & Lockman 1990) and a distance of M33 of 795 kpc (van den Bergh 1991), which we use throughout the paper.
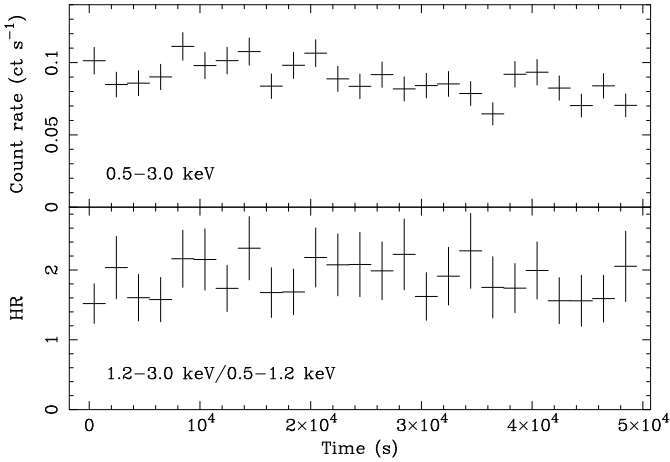

Fig. 2. *Chandra* ACIS I light curve and hardness ratio of M33 X−7 during observation 1730 integrated over 2000 s. Time zero corresponds to HJD 245 1737.88019 (solar system barycenter corrected). The light curves cover orbital phases 0.49–0.65 (ephemeris of D99).

we give raw count rate in Table 1, the light curves in Fig. 1 and 4 are corrected for vignetting and EPIC MOS count rates for the difference in instrument efficiency compared to EPIC PN (i.e. increased by a factor of 2.5). The vignetting corrections for far off-axis positions is up to a factor of 3.5 and may include systematic errors of up to 20%. The source extraction radii chosen assure that more than 80% of the PSF are covered. EPIC PN as well as MOS show X−7 at low intensity for XMM-Newton observations 0102640101 and 0102641101 which covered binary phase 0.01 to 0.16 according to the ephemeris of D99. During the other XMM-Newton observations (covering binary phase 0.18 to 0.85 according to the ephemeris of D99, see Fig. 1 and 4), the source was in high state. The high state intensity did not vary by more than ±20% between the observations. Within the observations the intensities changed by up to 30% on time scales as short as 1000 s (see Fig. 1). No significant variability in hardness ratio was detected between the observations. However, there seems to be variability on shorter time scales. Some of the observations suffer from strong particle background flares which show vignetting effects by the telescope mirrors. We did not exclude these times from the light curves but tried to correct by subtracting this variable background determined as close to X−7 as allowed by CCD configuration and emission from other nearby sources. Our selection of the background regions should minimize spurious effects on source count rate and hardness ratio. Nevertheless, residual effects may explain the count rate increase in observation 0141980701 around binary phase 0.55 seen in Fig. 4.

The light curve for the *Chandra* observation 1730 shows the source out of eclipse. While the count rate in the 0.5–3.0 keV band decreased during the observation by about 20% and
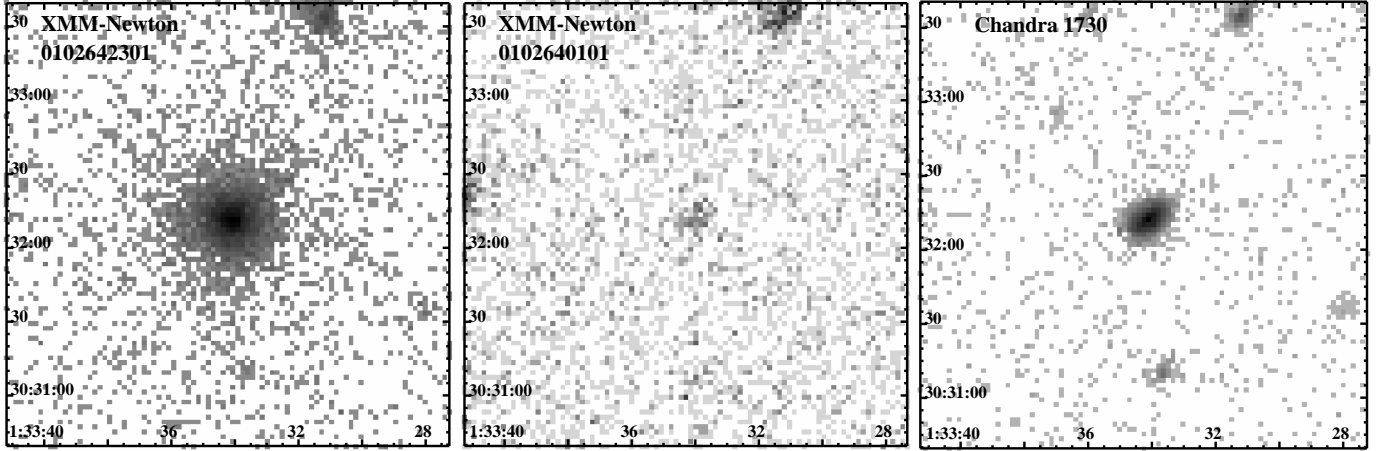
Fig. 3. Logarithmically-scaled, grey-scale images of the M33 X−7 region of the XMM-Newton EPIC observations 0102642301, 0102640101, and *Chandra* ACIS I observation 1730 (from left to right). The images (RA, Dec J2000.0) were accumulated with a pixel size of 2″, in the 0.5–4.5 keV band. EPIC PN and MOS images were selected for times of low background and added. Integration times for observation 0102642301 are 9.0, 12.1, and 12.2 ks for PN, MOS1, and MOS2, respectively, and the maximum in the image is 193 counts per pixel. The corresponding numbers for observation 0102640101 are 11.7, 10.6, and 12.4 ks and 12 counts per pixel. In this image M33 X−7 is close to a CCD gap in PN and there is no MOS exposure in the upper left corner of the image. For the *Chandra* image the integration time was 49.4 ks and the maximum in the image is 919 counts per pixel. M33 X−7 is the source in the center of the images and was in a low state (eclipse) during observation 0102640101. HP01 X67 is the source ∼ 1′.5 to the NNW of M33 X−7.

there is also variability down to the the sampling time scale of 2000 s, the hardness ratio did not change significantly (Fig. 2).

One has to keep in mind that the EPIC MOS count rates and HRs of X−7 can not directly be compared to the PN one as they originate from a CCD with a different energy response function. The same is even more true if one wants to compare *Chandra* and XMM-Newton count rates and HRs.

Figure 3 shows images (3′ to a side) of the X−7 area in the 0.5–4.5 keV band during the high and low state (XMM-Newton EPIC cameras are combined). X−7 is clearly detected also during the low state (∼ 3% of the average high state emission).

We searched for pulsations within the bright state XMM-Newton low background observations and the *Chandra* observation in the frequency range 10^{-3}–4 Hz following the Rayleigh Z_n^2 method (Buccheri et al. 1983) as described in Haberl & Zavlin (2002). No signal was found with more than 94% ($< 2\sigma$) confidence level. This includes the previously suggested period of 0.31 s (D99) although the time resolution of 0.073 s of the PN detector in the full frame mode may not be sufficient to clearly detect such a short period.

2.2. Improved position

HP01 give the position of X−7 with a 90% error radius of 2″.0 which is fully determined by the assumed remaining systematic error of 2″.0. The much higher number of photons detected with the *Chandra* ACIS I detectors and the good PSF even at an off-axis angle of 8′.6 allow us to determine a significantly improved source position in observation 1730. Systematic errors can be reduced by adjusting the positions using the well determined radio position of a supernova remnant (SNR) close to X−7 (source 57 in Gordon et al. 1999) which is also detected in X-rays (X67 in HP01), the X-ray source ∼ 1′.5 to the
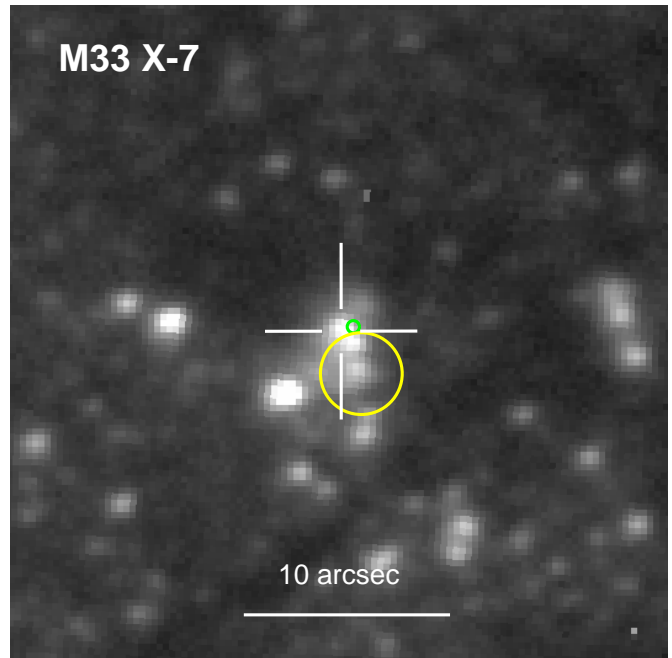

Fig. 5. Position of M33 X−7 is shown on a V image of the DIRECT survey. The ROSAT position and error from HP01 is marked by the big circle, *Chandra* position by the small circle. The optical identification, i.e. the star showing the 3.4 d variability, is marked by the cross hair.

NNW of X−7 in Fig. 3. We get a significantly improved position for X−7: α=01^{h}33^{m}34^s.21, δ=+30°32′11″.7 (J2000), with a remaining error radius of 0″.3 mainly determined from the statistical uncertainty of the X67 position.

Several XMM-Newton EPIC observations cover X−7 and in addition X67. The integration times of the individual observations are much shorter than for the *Chandra* observation and
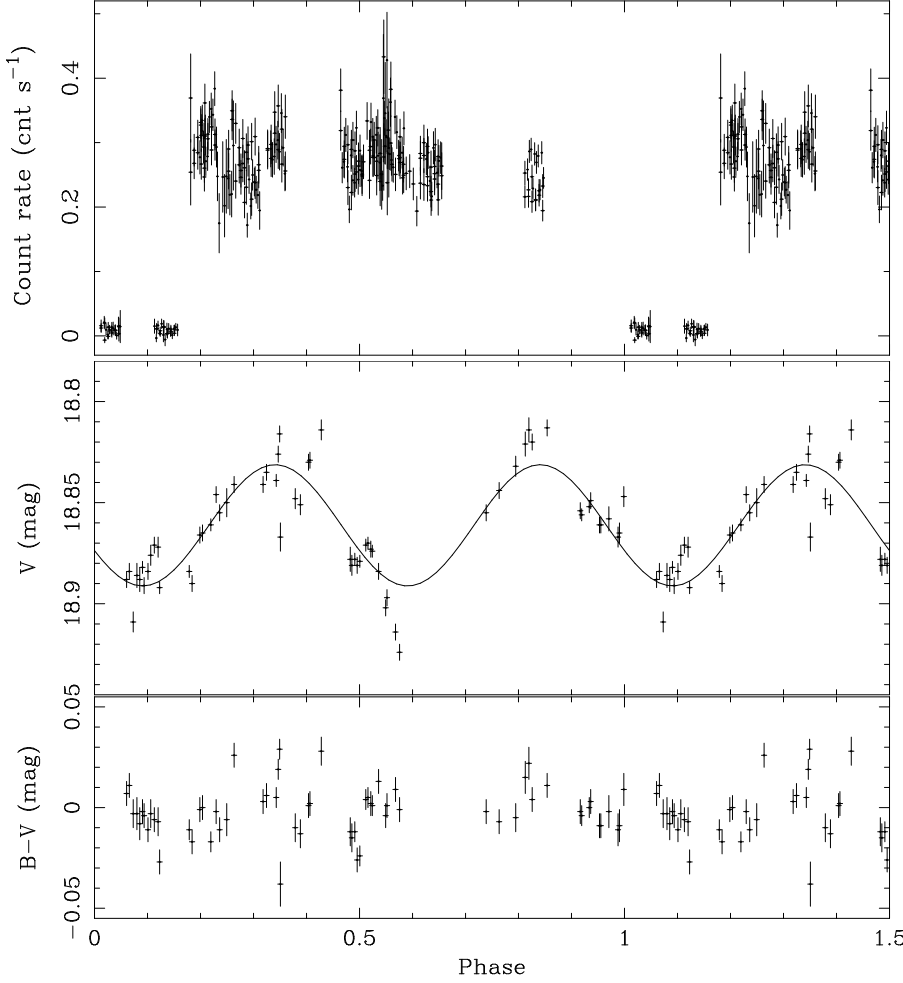
Fig. 4. Light curve of the XRB M33 X7 in the 0.5–3.0 keV band and in optical V and B-V folded over the 3.45 d orbital period using ephemeris of D99. Data for phase 0. to 0.5 are repeated at 1.0 to 1.5 for clarity. Added is a double-sinusoidal approximation to the V-data (full line, see text).

the XMM-Newton PSF is worse. XMM-Newton determined positions of X−7 have individual error radii of $1''0$ or greater for the PN and MOS cameras and are within the errors consistent with the *Chandra* position. See Fig. 5 for an overlay of the improved position on a deep optical *V*-band image.

2.3. Energy spectra

Spectra for the low background XMM-Newton EPIC observation 0102642301 and for the *Chandra* observation were approximated with simple spectral models (see Table 2). Individual EPIC PN and MOS spectra were simultaneously fitted with the same model parameters correcting for vignetting and the fraction of the PSF covered by the source extraction area. Energy independent normalization factors for each spectrum separately take into account possible differences in source coverage. Model components were the fixed Galactic foreground absorption plus additional absorption within M33 or in the immediate surrounding of the source using XSPEC model component WABS. A thin thermal (MEKAL) model could be rejected due to the high χ^2/ν, and also a power law (POWL) model still shows large residuals. Bremsstrahlung (BREMS) and also variable temperature disk blackbody (DISKBB) models on the other hand yield acceptable χ^2/ν values. We used the latter models to fit all high state observations of X−7 (see

Table 3). For all observations, absorbed BREMS or DISKBB models give acceptable fits. The BREMS model needs comparably high absorption outside the Galaxy. The model temperatures are the same within the errors. For the DISKBB model, on the other hand, the additional absorption is very low or absent and inner disk temperatures also don't vary significantly.

3. Optical observations and results

3.1. Observations

The data were obtained as part of the DIRECT project[1] (Mochejska et al. 2001a,c, M01b) at the Kitt Peak National Observatory[2] 2.1m telescope during two separate runs, from September 29th to October 5th, 1999 and from November 1st to 7th, 1999. The telescope was equipped with a Tektronix 2048 × 2048 CCD (T2KA camera) having a pixel scale $0.305''/pixel$. We collected 74×600 s exposures in the *V* filter and 30×600 s in *B*. The exposure times varied slightly to compensate for the changes of seeing conditions. The typical seeing was $1''5$.

[1] For information on the DIRECT project see http://cfa-www.harvard.edu/~kstanek/DIRECT/.

[2] Kitt Peak National Observatory is a division of NOAO, which are operated by the Association of Universities for Research in Astronomy, Inc. under cooperative agreement with the National Science Foundation.
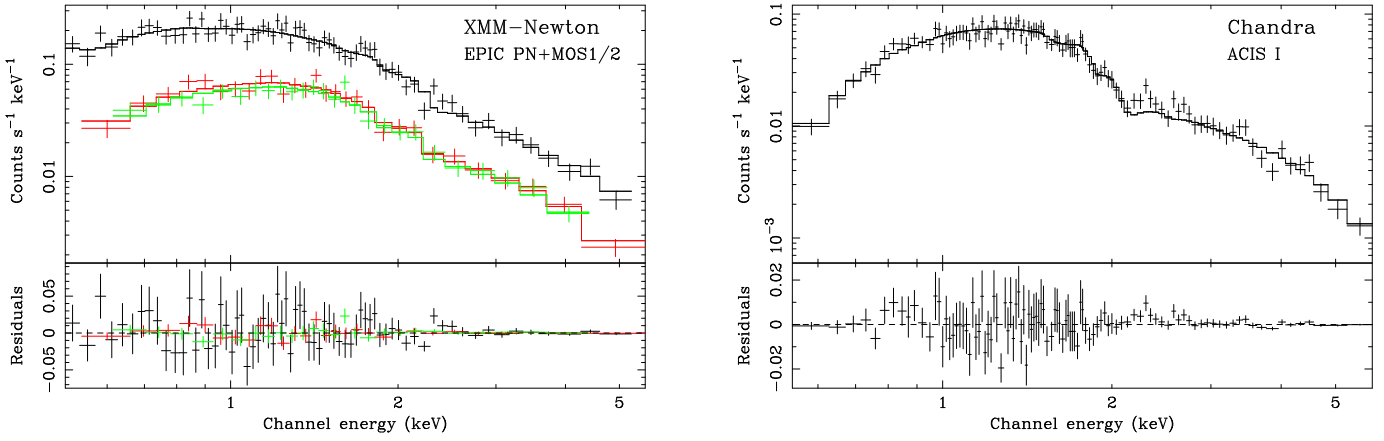
Fig. 6. M33 X−7 spectrum of XMM-Newton EPIC PN observation 0102641201 (left) and of *Chandra* ACIS I observation 1730 (right). Data and best fitting bremsstrahlung model are shown in the upper panels, residuals between data and model below. For the model parameters see Table 2.

Table 2. Spectral modeling results for M33 X−7 for the on-axis XMM-Newton EPIC observation 0102641201 (all EPIC instruments fitted together) and the *Chandra* ACIS I observation 1730. The degradation of the ACIS was taken into account using model *ACISABS* in XSPEC. For each instrument, we give the effective integration time T_{int} and the raw count rate. The number of energy bins reduced by the number of free parameters defines the degrees of freedom ν. In the case of $\chi^2/\nu \leq 2.0$, 90% errors are given.

Observation	Inst.	T_{int} (ks)	Raw count rate (10^{-2} ct s^{-1})	ν	Model[*]	$N_{H\,M33}$[**] (10^{20} cm^{-2})	Γ	kT (keV)	L_X[***] (10^{37} erg s^{-1})	χ^2/ν
XMM-Newton	PN	9.0	32.0±0.6	119	POWL	$19.3^{+3.1}_{-2.8}$	$2.24^{+0.09}_{-0.09}$		$6.9^{+0.6}_{-0.6}$	0.95
EPIC	MOS1	12.1	10.5±0.3		BREMS	$8.8^{+2.0}_{-2.0}$		$2.93^{+0.32}_{-0.27}$	$7.0^{+0.5}_{-0.5}$	0.79
0102642301	MOS2	12.2	9.2±0.3		THPL	$2.3^{+1.5}_{-1.4}$		$4.7^{+0.4}_{-0.2}$	$7.0^{+0.3}_{-0.3}$	1.47
					DISKBB	< 0.8		$0.96^{+0.04}_{-0.03}$	$7.1^{+1.0}_{-0.8}$	0.87
Chandra	ACIS I	49.4	10.2±0.2	101	POWL	$28.4^{+4.1}_{-3.8}$	$2.33^{+0.11}_{-0.08}$		$6.2^{+0.6}_{-0.6}$	1.23
1730					BREMS	$15.3^{+2.8}_{-2.6}$		$2.82^{+0.27}_{-0.24}$	$6.3^{+0.4}_{-0.4}$	0.98
					THPL	7.1		4.7	6.3	2.1
					DISKBB	$3.2^{+2.4}_{-2.3}$		$1.01^{+0.04}_{-0.05}$	$6.5^{+1.3}_{-1.1}$	0.97

[*] : THPL = thin thermal Plasma with solar abundance (XSPEC model MEKAL), BREMS = thermal bremsstrahlung, POWL = power law, DISKBB = disk blackbody
[**] : Absorption exceeding the fixed Galactic foreground
[***]: In the 0.5–4.5 keV band, corrected for Galactic absorption, corrected for extraction radii and vignetting

3.2. Data reduction and calibration

The preliminary processing of the CCD frames was performed with the standard routines in the IRAF ccdproc package.[3] The data were corrected for CCD non-linearity at this stage, as described by Mochejska et al. (2001a).

Photometry was extracted using the ISIS image subtraction package (Alard & Lupton 1998; Alard 2000). A brief outline of the method is presented here. For a more detailed description of the reduction procedure the reader is referred to Mochejska et al. (2001a).

The ISIS reduction procedure consists of the following steps: (1) transformation of all frames to a common (x, y) coordinate grid; (2) construction of a reference image from several best exposures; (3) subtraction of each frame from the reference image and (4) extraction of profile photometry from the subtracted images.

All computations were performed with the frames internally subdivided into four sections (`sub_x=sub_y=2`). Differential brightness variations of the background were fit with a second degree polynomial (`deg_bg=2`). A convolution kernel varying quadratically with position was used (`deg_spatial=2`). The PSF width (`psf_width`) was set to 15 pixels. We used a photometric radius (`radphot`) of 3 pixels.

Due to residual non-linearity, our photometry could not be calibrated from observations of standard stars. The coefficients for the color terms of the transformation were derived from the

---

[3] IRAF is distributed by the National Optical Astronomy Observatories, which are operated by the Association of Universities for Research in Astronomy, Inc., under cooperative agreement with the NSF.

Table 3. Spectral modeling results for the remaining out of eclipse XMM-Newton EPIC observations of M33 X−7 using thermal bremsstrahlung and disk blackbody spectra. In the last row, five EPIC PN spectra of low background observations (Σ EPIC PN; combining 0102640501, 0102640701, 0102642301, 0141980601, and 0141980801) are simultaneously fitted. Model parameters are given with 90% errors (see Table 2).

Observation	ν	Thermal bremsstrahlung $N_{\mathrm{H\,M33}}$ $(10^{20}\ \mathrm{cm}^{-2})$	kT (keV)	χ^2/ν	Disk blackbody $N_{\mathrm{H\,M33}}$ $(10^{20}\ \mathrm{cm}^{-2})$	kT (keV)	χ^2/ν
0102641201	53	$16.0^{+3.3}_{-3.3}$	$2.16^{+0.26}_{-0.22}$	0.79	$4.2^{+3.1}_{-2.8}$	$0.87^{+0.06}_{-0.05}$	0.96
0102640401	68	$12.3^{+3.1}_{-3.0}$	$2.66^{+0.33}_{-0.27}$	1.05	< 2.6	$0.99^{+0.04}_{-0.06}$	1.20
0102640501	53	$13.5^{+3.8}_{-3.6}$	$2.72^{+0.39}_{-0.33}$	1.00	< 4.6	$0.99^{+0.06}_{-0.06}$	0.99
0102640601^{+}	18	$11.4^{+10.4}_{-9.3}$	$2.87^{+4.29}_{-1.26}$	0.88	< 11.7	$0.90^{+0.25}_{-0.23}$	0.99
0102640701	41	$10.8^{+4.3}_{-4.0}$	$2.90^{+0.61}_{-0.47}$	0.91	< 3.3	$0.98^{+0.06}_{-0.07}$	0.93
0102642101*	30	$14.4^{+5.1}_{-4.6}$	$3.00^{+0.87}_{-0.61}$	0.97	< 8.4	$0.97^{+0.11}_{-0.10}$	0.97
0141980501	45	$12.7^{+4.6}_{-4.3}$	$2.54^{+0.48}_{-0.39}$	0.61	< 4.8	$0.94^{+0.07}_{-0.08}$	0.79
0141980601	75	$17.0^{+2.9}_{-2.7}$	$2.14^{+0.21}_{-0.18}$	1.25	$4.8^{+2.6}_{-2.4}$	$0.88^{+0.05}_{-0.05}$	1.15
0141980701	87	$9.4^{+4.1}_{-3.9}$	$2.83^{+0.89}_{-0.58}$	1.06	< 3.9	$0.90^{+0.08}_{-0.09}$	1.04
0141980801	80	$14.7^{+3.9}_{-2.8}$	$2.13^{+0.20}_{-0.17}$	1.01	< 4.4	$0.89^{+0.04}_{-0.05}$	0.92
Σ EPIC PN	251	$11.6^{+1.6}_{-1.5}$	$2.47^{+0.17}_{-0.15}$	1.07	< 1.7	$0.94^{+0.03}_{-0.03}$	1.04

Notes and references:

$^{+}$: M33 X−7 only in PN field of view.

* : M33 X−7 only in MOS field of view.

comparison of our NGC 6791 photometry with the data from the KPNO 0.9m telescope (Kaluzny & Udalski 1992). The offsets were determined relative to 735 stars above $V = 20$ mag from the DIRECT catalog of stellar objects in M33 (Macri et al. 2001). The calibration coefficients can be found in M01b.

The transformation from rectangular to equatorial coordinates was derived using 894 transformation stars with $V < 19.5$ from the DIRECT catalog of stellar objects in M33 (Macri et al. 2001). The average difference between the catalog and the computed coordinates for the transformation stars was 0.″06 in right ascension and 0.″06 in declination.

3.3. Results

We have searched within a radius of 36″ around the SIMBAD position of X−7 for stars with a period of around 3.45 d. From the 715 stars examined only one was a binary with a period of about 3.46-3.48 days. It is a star at position $\alpha = 01^{\mathrm{h}}33^{\mathrm{m}}34\overset{\mathrm{s}}{.}20$, $\delta = +30°32'11\overset{''}{.}08$ (J2000), with an average V magnitude of 18.86, and an amplitude of variation in this band of about 0.11 mag. From the images it seems to be located in a small star cluster (see Fig. 5). Measured V and B magnitudes are given in Table 4.

The binary light curve in the V band using the ephemeris of D99 (Fig. 4) shows two maxima and minima of different depth as expected for an ellipsoidal and X-ray heating light curve for a high mass XRB (HMXB) together with a double-sinusoidal fit to the data (average V magnitude of 18.862 ± 0.001, amplitude $(33 \pm 1) \times 10^{-3}$ mag). The phase of the shallower minimum is shifted by $+0.0956 \pm 0.0028$ with respect to the eclipse center of D99 in the same direction as also indicated by the X-ray light curve (see Sect. 2.1). The double-sinusoidal fit is only a crude approximation to the data and the model parameters certainly

are affected by non-uniform sampling of the optical light curve. The data suggest a deeper secondary minimum (around phase 0.6) which according to Tjemkes et al. (1986) might point at the effect of an accretion disk in the system. V magnitude and B–V color at X-ray eclipse are 18.890 and -0.005.

4. Discussion

4.1. Improved ephemeris

D99 determined the eclipse parameters for X−7 using in total 50 ks and 325 ks of archival ROSAT PSPC and HRI data, respectively, integrated over one satellite orbit (∼3 ks time bins). The XMM-Newton and *Chandra* low and high state observations of X−7 can naturally be explained by finding the source within and out of eclipse. Unfortunately, neither of the observations covered eclipse ingress or egress. However, from the XMM-Newton light curves we can deduce that the eclipse egress lasts < 0.02 and the ingress < 0.16 in phase (well within the parameter range given by D99). These values are only poorly determined due to gaps in the phase sampling over the orbit. More observations are needed to further constrain the binary ephemeris.

Nevertheless, we can restrict the time of eclipse egress to HJD $(245\ 1760.935 \pm 0.035)$ assuming that it is constrained by the end of observation 0102640101 (when X−7 is still in eclipse) and the beginning of observation 0141980501 (when, 261 binary orbits later, X−7 is already out of eclipse). With the eclipse shape parameters of D99 we then derive a mid-eclipse epoch of HJD $(245\ 1760.61 \pm 0.09)$. The new X-ray mid-eclipse time corresponds to binary phase 0.07 in Fig. 4. Combining this result with the mid-eclipse epoch of D99 we get an improved orbital period for X−7 of (3.45376 ± 0.00021) d well within the period errors given by D99.

4.2. The optical companion

The spectral classification of the optical companion can be deduced from the absolute optical magnitude and color during X-ray eclipse when we see the optical surface that is mostly undisturbed by gravitational effects, an expected accretion disk and heating by the X-ray source. To derive the absolute magnitude the measured brightness has to be corrected for the distance (-24.502 mag for the assumed distance of 795 kpc) and for interstellar extinction, the color has to be corrected for reddening. These corrections can be estimated from the Galactic N_H in the direction of X−7 as $A_{V\,Gal} = 0.36$ mag and $E(B-V)_{Gal} = -0.12$ (Predehl & Schmitt 1995). The N_H column depth of the M33 disk in the direction of X−7 is varying significantly on small scales. X−7 is not located in one of the H I holes catalogued by Deul & den Hartog (1990). The absorbing column within M33 can be determined to ~2.2×10^{21} cm^{-2} from a 47×93 arcsec half power beam width H I map (Newton 1980). The absorbing columns derived from the spectral fits to the X-ray spectra indicate half or less than this absorbing column depending on the spectral model. Assuming that we see X−7 through half of this column and that the same conversion applies as used above, we get $A_{V\,M33} = 0.62$ mag and $E(B-V)_{M33} = -0.21$. The companion star therefore should have an absolute V magnitude of -6.0 to -6.6 and $(B-V)_0$ of -0.12 to -0.33, which would correspond to a star of spectral typ B0I to O7I and masses M_2 of 25 to 35 $M_\odot$ (see e.g. Aller et al. 1982). Optical companions of similar spectral type were proposed by D99 based on binary orbit and eclipse length, assuming a 1.4 $M_\odot$ neutron star as the compact object.

4.3. M33 X−7, an eclipsing black hole XRB?

We can use the mass of the optical companion as determined in the previous subsection and the mass ratios determined from binary orbit and eclipse length (see D99 and Paczyński 1971; Eggleton 1983) to determine the mass M_X of the compact object. For a binary inclination of 90°, the mass ratio q$(= M_X/M_2)$ is 0.085 yielding M_X of 2.1–3.0 $M_\odot$, significantly higher than expected masses of neutron stars. For an inclination of 70°, q is 0.036 and $M_X = 0.9 - 1.2$ $M_\odot$ well in the range of typical neutron star masses. The inclination can not be constrained by our measurements and the mass estimates above do not exclude a neutron star for the compact object in the system.

Further information on the nature of the compact object may be infered from the X-ray spectrum. Before XMM-Newton and *Chandra*, the X-ray spectrum of X−7 was investigated using ROSAT and *Beppo*SAX observations. HP01 found that the X−7 spectrum in the ROSAT band can be described by an absorbed power law ($N_H = (1.9\pm0.9)\times10^{21}$ cm^{-2} and $\Gamma = 1.86 \pm 0.52$). Thin thermal plasma models did not give acceptable fits. Parmar et al. (2001) reported that *Beppo*SAX detected X−7 in the 2–8 keV band. The spectrum could be described equally well by a power law ($N_H < 9.8\times10^{22}$ cm^{-2} and photon index $\Gamma = 2.9^{+1.7}_{-1.3}$) or a Bremsstrahlung model ($N_H < 11\times10^{22}$ cm^{-2} and k$T = 3.7^{+97}_{-2.4}$). If the absorption is fixed to 5.6×10^{20} cm^{-2}, the power law photon index is constrained to 1.7±0.6 and the Bremsstrahlung temperature to

<3.7 keV. Keeping in mind the large uncertainties in the parameters, these results are consistent with the XMM-Newton and *Chandra* spectra reported for this persistent source in Sect. 2.3. In the following we therefore concentrate on these higher quality spectral results.

Thermal Bremsstrahlung and disk blackbody models yield acceptable fits to the XMM-Newton and *Chandra* spectra (see Sect. 2.3). For the first model an absorbing column comparable to half the H I values at the position of X−7 within M33 (see above) is needed to fit the X−7 spectra. The second model only allows us to determine upper limits for the M33 absorbing column in front of X−7 which are smaller than half the M33 column depth at that position. The X−7 X-ray spectra are steeper in the 2–10 keV band than typical for HMXB (flat power law shapes with photon indices of $0.8 < \Gamma < 1.5$, White et al. 1983) and better resemble the spectra of persistent black hole XRBs like LMC X−1 and Cyg X−1 (see e.g. Cui et al. 2002).

Therefore, the spectral results, our unsuccessful search for X-ray pulsations and the high mass estimate of the compact object, infered from the identified optical companion indicate a black hole as the compact object. These findings make M33 X−7 a very interesting source for further investigation as it could be the first eclipsing HMXB with a black hole as the compact object.

5. Conclusions

XMM-Newton and *Chandra* observations of the persistent eclipsing HMXB M33 X−7 allowed us to improve on the orbital period and investigate the X-ray spectrum in unprecedented detail. No X-ray pulsations were detected. A special investigation of the optical variability of DIRECT data of the region revealed in the optical the orbital light curve of a high mass companion. X-ray and optical data point at a black hole as the compact object in the system. Optical spectroscopy and high sensitivity X-ray pulsation searches are needed to clarify the situation.

References

Alard, C. 2000, A&AS, 144, 363

Alard, C. & Lupton, R. H. 1998, ApJ, 503, 325

Aller, L. H., Appenzeller, I., Baschek, B., et al., eds. 1982, Landolt-Börnstein: Numerical Data and Functional Relationships in Science and Technology - New Series " Gruppe/Group 6 Astronomy and Astrophysics " Volume 2 Schaifers/Voigt: Astronomy and Astrophysics / Astronomie und Astrophysik " Stars and Star Clusters / Sterne und Sternhaufen

Buccheri, R., Bennett, K., Bignami, G. F., et al. 1983, A&A, 128, 245

Cui, W., Feng, Y. X., Zhang, S. N., et al. 2002, ApJ, 576, 357

Deul, E. R. & den Hartog, R. H. 1990, A&A, 229, 362

Dickey, J. M. & Lockman, F. J. 1990, ARA&A, 28, 215

Dubus, G., Charles, P. A., Long, K. S., Hakala, P. J., & Kuulkers, E. 1999, MNRAS, 302, 731

Eggleton, P. P. 1983, ApJ, 268, 368

Gordon, S. M., Duric, N., Kirshner, R. P., Goss, W. M., & Viallefond, F. 1999, ApJS, 120, 247

Haberl, F. & Pietsch, W. 2001, A&A, 373, 438

Haberl, F. & Zavlin, V. E. 2002, A&A, 391, 571

Humphreys, R. M. & Sandage, A. 1980, ApJS, 44, 319

Jansen, F., Lumb, D., Altieri, B., et al. 2001, A&A, 365, L1

Kaluzny, J. & Udalski, A. 1992, Acta Astronomica, 42, 29

Larson, D. T. & Schulman, E. 1997, AJ, 113, 618

Liu, Q. Z., van Paradijs, J., & van den Heuvel, E. P. J. 2000, A&AS, 147, 25

Long, K. S., Dodorico, S., Charles, P. A., & Dopita, M. A. 1981, ApJ, 246, L61

Macri, L. M., Stanek, K. Z., Sasselov, D. D., Krockenberger, M., & Kaluzny, J. 2001, AJ, 121, 861

Markert, T. H. & Rallis, A. D. 1983, ApJ, 275, 571

Mochejska, B. J., Kaluzny, J., Stanek, K. Z., Sasselov, D. D., & Szentgyorgyi, A. H. 2001a, AJ, 121, 2032

—. 2001b, AJ, 122, 2477

—. 2001c, AJ, 121, 3284

Newton, K. 1980, MNRAS, 191, 615

Paczyński, B. 1971, ARA&A, 9, 183

Parmar, A. N., Sidoli, L., Oosterbroek, T., et al. 2001, A&A, 368, 420

Peres, G., Reale, F., Collura, A., & Fabbiano, G. 1989, ApJ, 336, 140

Pietsch, W., Ehle, M., Haberl, F., Misanovic, Z., & Trinchieri, G. 2003, Astronomische Nachrichten, 324, 85

Predehl, P. & Schmitt, J. H. M. M. 1995, A&A, 293, 889

Schulman, E., Bregman, J. N., Collura, A., Reale, F., & Peres, G. 1993, ApJ, 418, L67

—. 1994, ApJ, 426, L55

Strüder, L., Briel, U., Dennerl, K., et al. 2001, A&A, 365, L18

Tjemkes, S. A., van Paradijs, J., & Zuiderwijk, E. J. 1986, A&A, 154, 77

Trinchieri, G., Fabbiano, G., & Peres, G. 1988a, ApJ, 325, 531

—. 1988b, ApJ, 329, 1037

Turner, M. J. L., Abbey, A., Arnaud, M., et al. 2001, A&A, 365, L27

van den Bergh, S. 1991, PASP, 103, 609

Weisskopf, M. C., Tananbaum, H. D., Van Speybroeck, L. P., & O'Dell, S. L. 2000, in Proc. SPIE Vol. 4012, p. 2

White, N. E., Swank, J. H., & Holt, S. S. 1983, ApJ, 270, 711

Table 4. Optical light curve of the star identified with M33 X−7. Magnitude with error in the V or B filter (column F) and heliocentric Julian date (HJD) of the observation are given.

F	HJD − 2451400	Mag	F	HJD − 2451400	Mag
V	52.721458	18.854(4)	B	56.793912	18.887(4)
V	52.730637	18.856(3)	V	56.811296	18.884(4)
V	52.780012	18.852(3)	B	56.820741	18.873(4)
V	52.788819	18.849(4)	V	56.829560	18.876(5)
B	52.798183	18.852(3)	B	56.840301	18.865(4)
V	52.846146	18.861(4)	V	56.853021	18.871(4)
V	52.854931	18.861(4)	V	56.877454	18.872(5)
V	52.907662	18.858(6)	V	56.887141	18.892(3)
B	52.916632	18.856(5)	V	57.674028	18.867(7)
V	52.967407	18.867(5)	B	57.699340	18.829(8)
V	52.976493	18.865(5)	V	57.771528	18.848(5)
V	53.005012	18.847(5)	V	57.804664	18.851(5)
V	53.919248	18.841(4)	B	57.814074	18.838(4)
V	54.676273	18.878(6)	V	57.857789	18.830(4)
V	54.686343	18.881(5)	V	57.866620	18.829(4)
B	54.696771	18.866(3)	B	57.875891	18.831(4)
V	54.705671	18.878(3)	V	57.940764	18.814(5)
V	54.720822	18.881(4)	B	57.950278	18.842(4)
B	54.729942	18.855(3)	B	84.699097	18.873(3)
V	54.738519	18.879(3)	V	84.708727	18.884(3)
V	54.777199	18.871(3)	V	84.726852	18.890(4)
V	54.791528	18.870(3)	V	84.777234	18.866(4)
B	54.800428	18.875(3)	B	84.785775	18.865(4)
V	54.809769	18.873(4)	V	84.794618	18.865(4)
V	54.819468	18.874(3)	V	84.849259	18.861(3)
V	54.860521	18.884(4)	V	84.883831	18.846(4)
B	54.869780	18.897(4)	B	84.895440	18.844(3)
B	54.878403	18.898(4)	V	84.906539	18.855(4)
V	54.906435	18.902(4)	V	84.952697	18.850(7)
V	54.915324	18.897(4)	B	86.634097	18.853(3)
V	54.971019	18.914(4)	V	86.643438	18.855(4)
B	54.987986	18.923(4)	V	86.727384	18.844(4)
V	54.997303	18.924(4)	B	86.742824	18.837(4)
V	55.753866	18.832(5)	V	86.897975	18.821(6)
B	55.762789	18.827(4)	V	86.921400	18.814(6)
V	55.861551	18.820(4)	V	88.643009	18.841(4)
B	55.870822	18.824(3)	B	88.652106	18.843(3)
V	55.958808	18.813(4)	V	88.664965	18.835(4)
V	56.672176	18.888(4)	V	88.728738	18.839(3)
B	56.680891	18.895(3)	V	88.741968	18.826(4)
V	56.690012	18.884(4)	V	88.750914	18.816(4)
B	56.701400	18.883(3)	B	88.760104	18.845(2)
V	56.715382	18.909(5)	B	88.780637	18.824(3)
B	56.724583	18.906(4)	V	88.878808	18.826(6)
V	56.739606	18.886(6)	V	88.893958	18.830(7)
B	56.748368	18.883(5)	V	88.927685	18.813(7)
V	56.757824	18.888(6)	V	89.698310	18.912(4)
B	56.766597	18.880(4)	V	89.710938	18.912(3)
V	56.775752	18.882(3)	V	90.841655	18.838(5)
V	56.786528	18.891(4)	V	90.886076	18.835(6)